A numerical investigation of CO_2 gasification of biomass particles- Analysis of energy, exergy and entropy generation

Linwei Wang[1,2,3*], Ainul N. Izaharuddin[2], Nader Karimi[2,4], Manosh C. Paul[2*]

[1]Centre for Renewable Energy Systems Technologies (CREST), Wolfson School of Mechanical, Electrical and Manufacturing Engineering, Loughborough University, Leicestershire LE11 3TU, UK

[2]Systems, Power & Energy Research Division, James Watt School of Engineering, University of Glasgow, Glasgow G12 8QQ, UK

[3]Department of Thermal and Fluid Engineering, University of Twente, Drienerlolaan 5, 7522 NB, Enschede, the Netherlands

[4]School of Engineering and Materials Science, Queen Mary University of London, London E1 4NS, United Kingdom

*Corresponding author. Email: l.wang2@lboro.ac.uk; Manosh.Paul@glasgow.ac.uk.

Abstract

Much attention has been recently paid to biomass CO_2 gasification as a means of CO_2 utilisation and mitigation. In this study, a novel low-cost theoretical tool based on thermodynamic equilibrium, and a computational fluid dynamics model are developed to analyse gasification of biomass particles in a CO_2 atmosphere. It is shown that increases in C/CO_2 enhances the production of hydrogen and results in improving energy and exergy efficiencies of the process. In keeping with that reported for air gasification, increasing the moisture content of biomass intensifies hydrogen production and reduces the yield of CO. The effects of particle temperature on the gasification process are further explored through a spatiotemporal analysis of the gaseous chemical species. In particular, the results reveal that higher initial temperatures of biomass at the entrance of the reactor lead to stronger generation of chemical entropy. Also, the time trace of entropy generation is found to be affected significantly by the initial temperature of the biomass particle. Importantly, the relation between the particle temperature and total entropy generation is observed to be highly nonlinear. Further, it is found that the irreversibility of chemical reactions is the most significant contributor to the total entropy generation in the process.

Keywords: CO_2 biomass gasification, Biosyngas production, Energy and exergy efficiencies, Equilibrium and kinetic models, Unsteady entropy generation.

Nomenclature

A	pre-exponential factor	$\vec{V}$	diffusion velocity of the i^{th} species
C	Concentration	w	coefficient of H_2O in the global reaction
c	coefficients of gaseous products in the global reaction	X	mole fraction of species i
D_{im}	effective diffusion coefficient of the species i	x	composition of chemical element C
D_{ij}	binary diffusion coefficient for the $i-j$ species pair	Y	mass fraction of species i

$D_{T,i}$	thermal diffusion coefficient for the i^{th} species	y	composition of chemical element H
E_a	active energy	z	composition of chemical element O
E	entropy generation rate		
E_h	rate of entropy generation due to heat transfer	*Greek Symbols*	
E_m	rate of entropy generation due to mass transfer	ε	standard chemical exergy of species i
E_r	rate of entropy generation due to chemical reactions	η	cold gas efficiency
E_t	average entropy generation rate	φ	exergy efficiency
EN	energy	ξ	Energy efficiency
EX	exergy	λ	thermal conductivity
$\vec{f_i}$	body force per unit mass	ρ	density
HHV	higher heating value	μ_c	specific chemical potential
h	molar enthalpy of species i	ω	the rate of species i mass production per unit volume
K	equilibrium constant	χ	distribution coefficient of the volatile matter in biomass
k	reaction rate	Φ	viscous dissipation
LHV	lower heating value	σ	Rate of entropy generation per unit volume
$\overline{M}$	average molecular weight	ω_i	rate of species i mass production per unit volume
m	coefficient of CO_2 in the global reaction		
N	molar number of species i	*Subscripts*	
$\vec{q}$	heat-flux vector	b	biomass
R	ideal gas constant	ch	chemical
$\vec{s}$	entropy flux vector	gas	produced gaseous fuel
s	molar entropy of species i	i	i^{th} species
s_E	effective area of entropy generation	ph	physical
T	temperature	syn	syngas
t	time	sen	sensible
u	velocity		

1. Introduction

Biomass is regarded as a renewable energy source with growing expectations to meet the energy demands and contribute to the reduction of carbon dioxide emissions [1]. Research on biomass-to-energy conversion has experienced a significant growth in the past decades. Direct combustion and gasification are amongst the main technologies widely used to convert solid biomass resources into energy for heat and power generation [2][3]. Gasification is a thermochemical process that normally happens at around 800°C and produces gaseous fuels from solid feedstock by partial oxidation followed by reduction. The desired products of gasification are CO, H_2 and CH_4 and there are also co-produced gases such as N_2, CO_2 and other hydrocarbons (HC) [4][5].

Air [6], pure oxygen [7], steam [8] and mixtures of these [9] have all been used as biomass gasification agents in the conventional gasification processes. Similar attempts have been made on coal gasification [10][11]. Recently, due to the increasing significance of CO_2 utilisation and carbon capture and storage (CCS), biomass gasification using carbon dioxide (CO_2) as an oxidising agent has attracted much attention [12]. Biomass CO_2 gasification can be used as a compatible technology to support CO_2 mitigation. It is also based upon the fact that the reaction products from the gasification process mainly consists of CO and CO_2. A high concentration of CO_2 stream can be obtained through combustion of the produced gas with O_2 which can be easily sequestrated and/or recycled back to the gasifier as a gasifying agent [13]. The CO_2 gasification is, therefore, a promising and timely technology as it can play a direct role in greenhouse gas management. Further, carbon monoxide produced in CO_2 gasification can be used in many chemical processes in addition to the direct use in thermal energy production.

Much work has been conducted to investigate general gasification characteristics on the CO_2-enhanced gasification of biomass. Chen et al. [14] conducted experiments on biomass gasification under pure-air, air/steam and CO_2/O_2 atmospheres. They found that the higher heating values of the produced gases are generally greater when using CO_2/O_2 mixtures. Mathieu and his co-worker [15] investigated the influences of oxygen concentration and temperature of gasification medium on the gasification efficiency. They deduced that the gasification efficiency increases by about 4.5% when the mole fraction of oxygen was up from 21% to 40% or the temperature of gasifying agent varies from 298 K to 1098 K. Im-orb et al. [16] studied the gasification of rice straw in varying steam-CO_2 atmospheres numerically. The results indicated that the production of CO decreases continuously along with the increased CO_2/biomass ratio while the production of H_2 keeps nearly stable. Further, the increased CO_2/biomass ratio results in an increase in the cold gas efficiency. Jeremias et al. also found that the CO_2/biomass ratio has a significant effect on biomass gasification under CO_2/H_2O mixtures. The experiments conducted by Sadhwani et al. [17] also revealed that the carbon conversion rate is lower in biomass CO_2 gasification compared to that with oxygen gasification. Nonetheless, the conversion rate can be higher with increasing temperature in CO_2 gasification.

In addition to the thermo-chemical performance of gasification, the second law analysis of this process is of significance. Exergy analysis is an interdisciplinary concept that combines energy, environment, and sustainability and normally is applied for the process evaluation and improvement [18]. Ultimately, the efficiency of gasification process and the heating values of the produced syngas will be increased by determining the optimal operating conditions. This will result in the production of bio-syngas with good heating values that can be directly used for different downstream applications, while also providing an understanding of the sources of irreversibility. It follows that it is essential to understand both energy and exergy behaviours of biomass CO_2 gasification process.

Ptasinski et al. [19] compared the chemical and physical exergy efficiencies of syngas/produced gases from the gasification of coal and solid biofuels. They concluded that the solid biomass could be regarded as a high-quality fuel when the chemical exergy efficiency is considered. Karamarkovic et al. [20], conducted exergy and energy analyses of air gasification of biomass. These authors found that the gasification performance improved when the moisture content in the biomass fuel was lower. Further, the heat added into the gasification reactor intensified the production of CO and H_2 and decreased the amount of oxygen required for the complete gasification.

In general, the equilibrium model provides an approximation of the overall behaviour of the gasification system offering the advantage of low computational cost. The outcomes of this model can be further utilised in energy and exergy analyses of the process. Yet, the thermochemical process of biomass gasification also involves chemical kinetics and other complex phenomena and therefore require further investigations. In a gasification process [11], the heat from the hot surrounding gases and the thermal radiation from the walls of the reactor are absorbed by the particles to start the drying process in which the moisture content evaporates. This is followed by the devolatilisation process where the volatile matters release rapidly. Afterward, the volatiles and char react with oxygen and produce gaseous species. It is noted that the chemical reactions involved in the gasification process are in essence the same and hence independent of the model scaling. Therefore, it is necessary to establish the numerical model in the particle level to provide a deeper insight for the fundamental investigation of the thermochemical processes occurring in biomass gasification. Here, it should be also noted that the Lattice Boltzmann method applied in Rashidi et al [21][22][23] could be another interesting way to reveal heat transfer of the gasification process numerically.

Furthermore, entropy generation is central to the analysis of most thermo-mechanical and chemical systems [24]. In such systems, the sources of irreversibility are strongly coupled with heat transfer, mass transfer and chemical reactions [24]. Entropy is, therefore, a key thermodynamic property in irreversible processes such as combustion and gasification [26]. Entropy generation has been widely used to provide understanding and a means of optimisation in thermal and thermochemical processes [25]. Entropy generation has been widely used to provide understanding and a means of optimisation in thermal and thermochemical processes [26][27]. So far, most studies about entropy generation in thermochemical processes have been focused on the combustion of gaseous fuels or the behaviour under a steady state condition [28][29]. In fact, to the best of authors' knowledge, currently there is no investigation on the transient entropy generation during biomass particle gasification. This concept can be potentially applied to the analysis of CO_2 gasification as a means of optimisation.

Therefore, a systematic fundamental analysis of the biomass gasification process in CO_2 atmosphere has been less extensively studied. In order to obtain a deeper understanding of this process, the general objective of the study is to carry out a detailed investigation of biomass CO_2 gasification of biomass based on the first and second law of thermodynamics. In particular, the syngas production, energy and exergy efficiencies and thermodynamic irreversibility of the process are examined. The work includes development of a thermochemical equilibrium model of gasification followed by predicting the unsteady evolution of the gaseous species through utilising a computational fluid dynamics (CFD) model. The entropy generation rates due to different factors and the resultant loss of exergy are further calculated.

2. Methodologies

2.1 Thermochemical equilibrium model

Due to the very low levels of nitrogen and sulphur substances based on the ultimate analysis, biomass feedstock can be described as $C_xH_yO_z$ for the development of this model [30][31]. Therefore, the global gasification reaction is expressed as follows:

$$\mathrm{C_xH_yO_z + wH_2O + mCO_2 \rightarrow c_1H_2 + c_2CO + c_3CO_2 + c_4H_2O + c_5CH_4} \quad (1)$$

where w and m are the amount of water and carbon dioxide per mol of biomass fuel, respectively, and c_1, c_2, c_3, c_4 and c_5 are the coefficients of the gaseous products. The three independent reactions coupled with the global reaction in the equilibrium model are given by the followings.

$$\mathrm{C + 2H_2 \rightarrow CH_4} \quad (2)$$

$$\mathrm{CO + H_2O \rightarrow CO_2 + H_2} \quad (3)$$

$$\mathrm{C + H_2O \rightarrow CO + H_2} \quad (4)$$

Based on the elemental balance and equilibrium constants, the coefficients of gaseous products could be found. That is:

Carbon balance: $x + m = c_2 + c_3 + c_5$ (5)

Hydrogen balance: $y + 2w = 2c_1 + 2c_4 + 4c_5$ (6)

Oxygen balance: $z + w + 2m = c_2 + 2c_3 + c_4$ (7)

Equilibrium constants [32]:

$$\mathrm{K_1 = [CH_4]/[H_2]^2 = c_5/c_1^2} \quad (8)$$

$$\mathrm{K_2 = [CO_2][H_2]/[CO][H_2O] = c_1c_3/c_2c_4} \quad (9)$$

$$\mathrm{K_3 = [CO][H_2]/[H_2O] = c_1c_2/c_4} \quad (10)$$

The general assumptions made in developing all equilibrium models are [33]: a) the gasifier is perfectly mixed and the temperature is uniformly distributed, b) all the chemical reactions have sufficient time to reach the equilibrium state, c) the pathways and formation of any intermediates are not considered, d) tar and soot formation are excluded.

2.2 Exergy and energy analysis

The cold gas efficiency of the gasification process is defined as [34],

$$\eta = \frac{N_{gas}\, LHV_{gas}}{m_b LHV_b}, \tag{11}$$

where N_{gas} is the molar amount of the product gas, m_b is the mass of the biomass feedstock, LHV_{gas} and LHV_b are the lower heating values of the product gas and biomass fuel, respectively. These values can be calculated by the following equations [20][35]:

$$LHV_{gas} = 282993X_{CO} + 241827X_{H_2} + 802303X_{CH_4}, \tag{12}$$

$$LHV_b = (HHV_b - 219.2H)(1 - w/100) - 0.2453w, \tag{13}$$

$$HHV_b = 349.1C + 1178.3H - 103.4O, \tag{14}$$

where X_{CO}, X_{H_2} and X_{CH_4} are the mole fraction of species CO, H_2, and CH_4 in the product gases, respectively. Further, C, H and O are the mass fraction for carbon, hydrogen, and oxygen in the biomass feedstock, respectively.

The exergy efficiency of the gasification process is defined as [19]:

$$\varphi = \frac{EX_{ch,gas} + EX_{ph,gas}}{EX_b}, \tag{15}$$

where $EX_{ch,gas}$ and $EX_{ph,gas}$ are the chemical and physical exergy of the product gas respectively, and Ex_b is the exergy of the biomass fuel. These are calculated by the following relations [36]:

$$EX_{ch,gas} = \sum_i N_i X_i \varepsilon_{0i} + RT_0 \sum_i N_i X_i ln X_i, \tag{16a}$$

$$EX_{ph,gas} = \sum_i N_i \left[\left(h_i - h_{0_i}\right) - T_0\left(s_i - s_{0_i}\right)\right], \tag{16b}$$

$$EX_b = \frac{1.044 + 0.016 \cdot \frac{H}{C} - 0.3493 \cdot \frac{O}{C} \cdot \left[1 + 0.0531 \cdot \frac{H}{C}\right]}{1 - 0.4124 \cdot \frac{O}{C}} \times LHV_b \tag{17}$$

where N_i is the molar number of species i, X_i is the mole fraction of species i, ε_{0i} is the standard chemical exergy of species i (the values are given in Table 1), R is the ideal gas constant, T_0 is the reference environmental temperature, h, and s are the molar enthalpy and entropy of species i.

Table 1. Standard chemical exergy for each component [37]

Gas species	Standard chemical exergy ($kJ/kmol$)
CH_4	8.32×10^5
CO	2.75×10^5
CO_2	1.99×10^4
H_2	2.36×10^5
H_2O	1.99×10^4
N_2	7.20×10^2

Here, we focused on the exergetic efficiency of the process. More information about the global exergy balance could be found in Ref. [36].

The energy balance of the gasification process can be written as [36]:

$$EN_b + EN_{CO_2} = EN_{syn} + EN_{sen} + EN_{loss}. \quad (18)$$

Here, we have [36]:

$$EN_b = m_b LHV_b \quad (18a)$$

$$EN_{CO_2} = m \cdot \int_{T_0}^{T_{syn}} C_{p,CO_2} T dT \quad (18b)$$

$$EN_{syn} = N_{syn} \cdot LHV_{gas} \quad (18c)$$

$$EN_{sen} = N_{syn} \cdot \sum_i X_i \cdot \int_{T_0}^{T_{syn}} C_{p,i} T dT \quad (18d)$$

where N_{syn} represents the molar number of the syngas.

Thus, the energy efficiency is defined as

$$\xi = 1 - EN_{loss}/EN_b \quad (19)$$

in which, EN_b, EN_{CO_2}, EN_{syn}, EN_{sen} and EN_{loss} are the energy in biomass fuel, injected CO_2 agent, product syngas, sensible and loss, respectively. It should be pointed out that, as the equilibrium model focuses on the theoretical syngas production from the feedstock and the gasification temperature is fixed in the model, the calculation of efficiencies is regardless of the energy consumed by the gasification equipment.

The exegetic analysis based on the equilibrium model serves as an approximation tool for performance evaluation and optimisation of the process. This is due to the simplifying assumptions embedded in the developed equilibrium model. More accurate outcomes are expected from the detailed numerical analyses that will be described in the following section.

2.3 Numerical scheme and gasification model

As stated, a numerical model was developed to simulate the biomass gasification under the CO_2 environment at the particle scale. The CFD model used for the biomass particle simulation was extensively introduced and rigorously validated in Refs. [3][38][39]. Therefore, for conciseness reasons, here only a summary of the model is provided briefly.

The considered configuration and the employed computational grid are shown in Fig. 1. The physical system includes a cylindrical tube full of CO_2 and subject to the carefully controlled thermal boundary condition [38][39]. The gaseous medium inside the reactor has a uniform initial temperature. A biomass particle is released from the top of the cylinder and it travels down along the centreline by the action of gravity while disturbing the surrounding gases. The following assumptions were made throughout the

simulations: a) the biomass particle is spherical, b) the gaseous atmosphere is assumed to be an ideal-gas mixture, c) the configuration is axisymmetric, d) tar and soot formation are ignored. The governing equations (mass, momentum, energy and species) along with the pertinent boundary conditions can be found in Ref. [39] and are not further discussed here. The numerical modelling was conducted taking a Euler-Lagrange approach coupled with the weighted-sum-of-grey-gases model (WSGGM) and the P-1 radiation model. Turbulence was incorporated through using a standard k-epsilon model. SIMPLE algorithm was implemented for the velocity-pressure coupling. The simulations were run on ANSYS FLUENT [40]. A second-order scheme discretisation scheme was applied to ensure high accuracy, and the convergence standard was set to 10^{-6} for energy and radiation calculations, and 10^{-4} for others. An extensive study on the grid independency was conducted with the computational cells varying amongst 18950, 29925, 37710 and 52680. The grid density with 29925 cells was applied in this work. The operating conditions used in this study are listed as below:

Table 2. Operating conditions.

Parameters	Values
Temperature of the gasification reactor	1000 K
Temperature of the injected gas	1000 K
Velocity of the injected gas	4.55 cm/s
Temperature of the injected particle	300 K, 500 K, 800 K, 1000 K
Initial diameter of the particle	80 μm
Initial velocity of the particle	15 cm/s

It is important to note that the comprehensive chemistry of the current problem is exceedingly complex and therefore using a simplified chemical mechanism is a necessity. In choosing such mechanism, priory was given to the reactions that dominate syngas production and thus could predict composition of the produced gas with good accuracy. In the current study, the single rate model is used to simulate the volatile releasing process. It is assumed that the devolatilisation is a first-order reaction [41]. The reaction and pertinent kinetics rate that employs global kinetics are given by:

$$\boldsymbol{R1}: biomass \rightarrow \chi\, Volatile + (1-\chi)\, Char, \tag{20}$$

$$k_1 = A_1 exp(-E_{a1}/RT), \tag{21}$$

where χ defines the amount of the volatile matter in the feedstock. The pre-exponential factor and activation energy of this devolatilization reaction are taken as $3.12 \times 10^5\, s^{-1}$ and $7.4 \times 10^7\, J/kmol$, respectively [41].

The reaction of char under CO_2 atmosphere yields carbon monoxide (CO) through the following heterogeneous reaction of gasification [42]:

$$\boldsymbol{R2}: C_{(s)} + CO_2 \rightarrow 2\, CO, \tag{22}$$

$$k_2 = A_2 T exp(-E_{a2}/RT) \cdot C_{c(s)} \cdot C_{co_2}, \tag{23}$$

Further, the pre-exponential factor and activation energy are taken as 4.4 s^{-1} and $1.6\times10^{8}\ J/kmol$ in this reaction, respectively [42].

2.5 Gas-phase entropy generation

The rate of entropy generation is derived from the governing equations by applying Gibbs equation. For maintaining conciseness, the complete derivation of entropy generation calculation is not shown here, as it has been reported, in length, in the previous works of the authors [38][39]. In summary, the rate of entropy generation due to heat transfer (E_h), mass transfer (E_m), and chemical reactions (E_r) are presented as follows.

$$E_h = \frac{\lambda}{T^2}(\nabla T)^2, \tag{24a}$$

$$E_m = \frac{\rho R D_{im}}{\bar{M}} \sum_i \frac{1}{X_i}(\nabla X_i)^2, \tag{24b}$$

$$E_r = -\frac{1}{T}\sum_i \mu_{c,i}\omega_i. \tag{24c}$$

Here, T is the gas-phase temperature, λ defines the thermal conductivity of the gas, ρ is the gas density, R is the gas constant, D_{im} represents the effective diffusion coefficient of the species i, $\overline{M}$ is the average molecular weight, X_i is the mole fraction of species i, μ_c denotes the specific chemical potential and ω_i is the mass production rate of species i per unit volume. Further information about the entropy generation in the investigated reactive medium is provided in Appendix A.

Eqs. (24) represents the rate of entropy generation per unit area. Therefore, the instantaneous entropy generation rate in the entire system can be found integrating the rate of entropy generation per unit volume over the effective area where gasification happens (s_E):

$$E_{whole} = \int E ds_E, \tag{25}$$

in which s_E is the effective area of thermodynamic irreversibility.

Lastly, by integrating and dividing the system entropy generation rate over the total time of the gasification process, the time averaging entropy generation is expressed as:

$$E_t = \frac{1}{t_{end}}\int_0^{t_{end}} E_{whole} dt. \tag{26}$$

The calculations of entropy generation were post-processed in a routine coded in MATLAB, and the data required were extracted from the CFD solver.

3. Validation

Materials from Refs. [43][44] were chosen as the biomass feedstock to validate the equilibrium model presented in Section 2.1. The basic chemical properties of these feedstock are listed in Table 3.

Table 3. Ultimate analysis of cardboard sample (%)

Materials	C	H	O	N	Others	Ref
Cardboard	44.02	5.83	44.56	0.37	0.22	[43]
RS-550	48.73	2.21	46.23	1.35	1.48	[44]
CC	67.50	0.75	29.81	0.47	1.47	[44]

Further, a mainstream equilibrium model "GasEq" [32] that has been widely used for biomass gasification with air was introduced and compared with the numerical predictions. Here, the new equilibrium model proposed in this study is named "NEM".

The comparison of the mole fraction of species H_2 and CO in the product gases between the experiments and the simulation results from the equilibrium models is shown in Table 4 (Here $Error = (|Numerical\ result - Experimental\ result|)/Experimental\ result$). It can be clearly seen that the new equilibrium model "NEM" proposed in this study predicts the experimental results well. It features a good match with the experimental data while the cited GasEq model [32] shows lack of accuracy. This discrepancy indicates that switching from air to carbon dioxide as the gasification agent requires modification of the equilibrium model. Approximate nature of the developed equilibrium model introduces certain level of error. Also, excluding minor chemical elements, such as nitrogen and sulfur, in the biomass feedstock leads to further error. Despite these, the error margin of the presented model remains within an acceptable level. Therefore, it can be concluded that the equilibrium model is valid and can support the parameter sensitivity analysis.

Table 4. The comparison among experimental data and equilibrium models.

Materials	Species	Experimental Data (%)[43][44]	NEM (%)	Error	GasEq (%)	Error
Cardboard	H_2	10.2	8.7	0.14	2.3	1.31
	CO	27.6	27.3	0.01	45.2	0.44
RS-550	H_2	7.1	5.7	0.19	1.8	0.75
	CO	45.3	47.1	0.04	35.8	0.21
CC	H_2	1.2	0.9	0.25	0.5	0.66
	CO	21.5	24.3	0.13	31.7	0.47

Further, the computational model proposed in Section 2.2 has been rigorously validated in simulating the single coal and biomass particle combustion process under various CO_2 environments, see [3][38][39] for the details. Due to the similarities between combustion and gasification of a single biomass particle, the validated CFD model is used here to simulate the transient gasification process in CO_2 atmosphere.

4. Results and Discussion

4.1 Gasification performances

The syngas production and gasification efficiencies are known to be affected by the feedstock type, gasification agent and gasification temperature [45][46]. In this study, the effects of varying the moisture content of feedstock, C/CO_2 ratios and gasification temperatures upon the performances of the gasification process are investigated. Here, the C/CO_2 ratio is defined as the molar ratio of the total amount of carbon in the biomass fuel to the total amount of CO_2 injected into the gasifier.

The effects of moisture content and C/CO_2 ratio on the syngas production when the gasification temperature is fixed at 1000K are shown in Fig. 2. It can be seen in Fig. 2a that as the moisture content in the feedstock increases, the mole fraction of H_2 in the produced gas increases slightly. However, in the meantime, production of CO drops from 35% to 28%. Further, the results indicate that the higher content of moisture in biomass does not promote the production of CH_4 and, consumption of CO_2 remains nearly indifferent to biomass moisture content. When considering the changes in C/CO_2 ratio (Fig. 2b), it is obvious that the concentration of CO and CO_2 in the product gases feature the opposite trend. There are more CO generated as the product and less CO_2 remaining as the gasification agent when the C/CO_2 ratio increases. The inverse changing trend of carbon dioxide and carbon monoxide can be attributed to the chemical reactions between the carbon and the gasifier agent - carbon dioxide through Boudouard reaction: $C + CO_2 \rightarrow 2CO$. Further, the amount of H_2 in the products shows an increase along with the growth in the C/CO_2 ratio. However, the generation of CH_4 is not noticeably affected by the variations in C/CO_2 ratio and the mole fraction of CH_4 is almost constant at a very low level (1%-1.8%) with the C/CO_2 ratio variation.

The lower heating value (LHV) of the produced syngas and the gasification efficiencies are calculated to present the gasification system performance under different conditions. Here, the gasification temperature is fixed at 1000K, and the cold gas efficiency, exergy efficiency, and energy efficiency are calculated. Figure 3a indicates that the lower heating value of syngas slightly decreases when the moisture content in the feedstock varies from 0% to 20%. This is because the carbon monoxide that has a higher heating value accounts for fewer percentages in the syngas when the feedstock has a higher moisture content (Fig. 2a). Similarly, the cold gas efficiency, exergy efficiency, and energy efficiency all present the downward trend. More specifically, the cold gas efficiency has a small decrease from 65% to 60%, the energy efficiency from 55% to 50% and the exergy efficiency from 43% to 39%. The higher moisture content in the feedstock absorbs more heat during the gasification process and results in lower efficiencies. However, as shown in Fig. 3b, the influence of the C/CO_2 ratio on the biomass gasification is much more noticeable. The lower heating value of the produced syngas rises by 30% from 230 kJ/kmol to 300 kJ/kmol when the C/CO_2 ratio increases from 0.31 to 0.52, which corresponds to the component variations of the gas mixture in the syngas (Fig. 2b). Further, the gasification

efficiencies have an upward trend as well. This is because the mole fractions of the main components, i.e. CO and H_2, in the syngas are larger for higher C/CO_2 ratios.

Different gasification temperatures are considered in this study. Figure 4 shows the effects of varying C/CO_2 ratio on the H_2 and CO production, CO_2 reduction and gasification efficiencies for the gasification temperature varying from 900K to 1200K. Here, the CO_2 reduction rate is defined as the ratio between the amount of CO_2 consumed during the gasification process and the amount of CO_2 supplied to the system. In addition, the carbon conversion rate is defined as the ratio of the amount of carbon contained in the syngas and the amount of carbon in the feedstock.

Firstly, Fig. 4a compares the mole fraction of hydrogen in the syngas under different gasification temperatures and C/CO_2 ratios. Evidently, for any fixed value of C/CO_2 ratio, an increase in the gasification temperature contributes to a decrease in the production of hydrogen. While under the same gasification temperature, the yield of hydrogen rises as the C/CO_2 ratio increases. Further, Fig. 4b reports the results of CO production in the syngas under different gasification conditions. Interestingly, the mole fraction of CO in the syngas shows the opposite trend to that of hydrogen. The higher the gasification temperature and the higher the C/CO_2 ratio, the more yield of CO is gained.

The results of the CO_2 reduction rate and carbon conversion rate under varying gasification temperatures and C/CO_2 ratios are presented in Figs. 4c and 4d, respectively. These figures indicate that the CO_2 reduction rate and the carbon conversion rate inflate when the gasification temperature or the C/CO_2 ratio increases. This implies that a larger fraction of CO_2 is consumed and converted into carbonaceous compounds (CO and CH_4) in the products. Meanwhile, the trends of the reduction and conversion rate also supports the results shown in Fig. 4b in which the mole fraction of CO in the syngas becomes higher along with increasing the gasification temperature or the C/CO_2 ratio. It also indicates that an increase in the gasification temperature promotes the chemical reactions related to CO production. Nevertheless, for the water-gas shift reaction ($CO + H_2O \rightarrow CO_2 + H_2$), the conversion of reactants to products becomes less favourable with increasing temperature due to the exothermic nature of this reaction. This explains the decrease in the amount of hydrogen observed in Fig. 4a.

The calculated cold gas efficiency and exergy efficiency of the gasification system are reported in Figs. 4e and 4f, respectively. It is inferred from these figures that the two efficiencies have the same changing trend. The efficiencies increase when the gasification temperature or the C/CO_2 ratio grows. Further, corresponding to the CO_2 reduction and carbon conversion rate in Figs. 4c and 4d, it can be concluded that the system performance is superior under higher temperatures and higher C/CO_2 ratio conditions. These results clearly demonstrate an important challenge faced by the CO_2 gasification of biomass. Addition of CO_2 (or dropping the numerical value of C/CO_2) results in the decline of gasification

efficiencies and thus makes the process more difficult. It is therefore imperative to carefully optimise the process of CO_2 gasification of biomass. In the rest of this section, the local and total generation of entropy during gasification process are explored to provide an insight into the mechanisms of irreversibility and inefficiencies.

It is important to note that the energetic and energetic efficiencies are fundamentally different measures of process performance [24][25]. It is therefore impossible to infer the behaviour of one by having a knowledge of the other. Hence, the qualitative similarity between the energy and exergy efficiencies in this section is a case-specific result and should not be generalised beyond the current analysis.

4.2. Spatiotemporal evolutions

The temporal evolution of the gas temperature, the mole fractions of CO, CO_2 and volatile in a part of the reactor close to the falling particle were predicted by the CFD model. The temperature of the gasification reactor was fixed at 1000K for all simulations. The cases with the biomass particle temperature at 500K and 1000K were selected for presentation in Figs. 5 and 6, respectively. A near-particle window is used to present the results as chemical activities and the heat and mass transfer occur in the vicinity of the single biomass particle. All the sub-figures have the same dimensions. The investigation commences from a moment prior to the start of char reaction and the time intervals between them have been maintained constant.

Figures 5a and 6a illustrate the spatiotemporal variations of the gas-phase temperature around the biomass particle during gasification. There are no significant differences in these sub-figures, which means the temperature of the gas surrounding the particle has not changed much during the whole process. This is because only one single particle was injected into the reactor and the reactor was heated to maintain a stable temperature. Further, the temperature differences caused by the gasification reactions are quite small and the effects of the endothermic devolatilisation and Boudouard reactions are not noticeable. Compared with the combustion of biomass and coal particles [38][39], the gas-phase temperature variations during gasification are less obvious. It will be later shown that this affects the generation of thermal entropy in the gasification process and makes it distinctive to that in the corresponding combustion process.

In a sharp contrast to that of the temperature fields, the unsteady variations of the major chemical species are quite noticeable. The formation and transport of carbon monoxide (CO) at the particle temperature of 500K are depicted in Fig. 5b. There is no CO appearing in the leftmost subfigure representing 130ms after the particle release. This is because the CO is generated through the char reaction (R2) which occurs about 150ms after the particle injection. A small cloud of CO around the biomass particle is

observed later. The growth of this cloud around the particle in the subfigures represents the increase in the amount and concentration of CO as the gasification process and chemical reactions progress.

Figures 5c and 5d show the unsteady evolutions of the species volatile and carbon dioxide (CO_2). The volatile matter is released into the environment when the single biomass particle drops into the reactor and the devolatilisation reaction (R1) takes place. The amount of volatile accumulates and spreads to a larger area with time elapsing. It should be pointed out that, the contours of CO_2 and volatile concentration are in a unity of opposites. The contours in which CO_2 has a lower concentration correspond to the cases where volatile has a higher concentration. This is because, in the current gasification model, the gaseous species are CO_2, CO and volatile. As a pure CO_2 environment is applied during the single biomass particle gasification process, the amounts of CO and volatile are very small compared to CO_2. Further, the concentration of CO is much lower than that of the volatile matters. Therefore, the clouds representing CO are negligible when looking into the concentration distribution of CO_2 and volatile.

The unsteady evolutions of the gaseous species CO, volatile and CO_2 when the biomass particle temperature is 1000K are reported in Figs. 6b, 6c, and 6d, respectively. Similar to that under 500K (shown in Fig. 5), the subfigures represent the unsteady evolutions of these species under the biomass gasification process. CO is generated until the char reaction is activated (85ms) and the peak concentration is around the particle as a result of reaction (R2). The volatiles appear once the particle is released into the reactor and the volatile matters in the reactor become evenly distributed due to their continuous diffusion to the surroundings. A close inspection of Figs. 5 and 6 further reveals that the initial temperature of the biomass particle has a non-trivial effect on the gasification process. The appearance time and concentration of the gaseous species indicate that the occurrence of gasification reactions is promoted and the rates of chemical reactions are accelerated at the higher temperature for both devolatilisation and Boudouard reactions. Further, it is obvious that the positions of the particle and concentration fields are much further away from the releasing point in the downward direction. This is a consequence of different gravity and buoyancy forces acting on different chemical species. A lengthy discussion of these effects can be found in the previous works of the authors on combustion of biomass in a CO_2 rich atmosphere [38][39].

4.3 Unsteady entropy generation

The average rate and the unsteady evolutions of entropy generation during the gasification process under the varying initial temperature of the particle are illustrated in Figs. 7-10. The average rate of entropy generation due to heat transfer, mass transfer, and chemical reactions are calculated by time-averaging the integrated entropy generation. It is worth noting that in the current problem, the frictional irreversibility is negligibly small and is therefore excluded. Figure 7 shows the results of these

calculations. Here, the time interval considered for the averaging is 280ms after the particle drops. This figure demonstrates that the irreversibility encountered by the chemical reactions is the most significant contributor to the total entropy generation amongst the three identified sources of irreversibility (i.e. chemical, thermal and mass transfer irreversibility). This is in keeping with that found in a combustion of single coal or biomass particle combustion [38][39]. The irreversibility due to heat transfer accounts for the least entropy generation, especially for the case in which the particle temperature is set to 1000K. This is, of course, very different to that observed in gas-phase combustion process for which thermal irreversibility is often a major source of entropy generation [39][47][48]. Further, the entropy generation rates by both mass transfer and chemical reactions rise when the particle temperature increases. This is due to the fact that the chemical reaction rates are higher, and the amounts of reaction products are bigger under higher temperature conditions. Further, there is a growth in the chemical entropy when the particle temperature increases from 500K to 800K. However, due to the smaller temperature gap between the particle and the surroundings, the generation rate of thermal entropy drops accordingly as the particle temperature increases. Figure 7 implies that, in general, the relation between particle temperature and entropy generation is highly nonlinear. This is mainly due to the very strong temperature dependency of the chemical entropy generation. It is noted that while this quantity does not change considerably between 300K and 500K, an increase of temperature to 800K causes a major inflation in the generation of entropy through the chemical mechanism.

Figure 8 shows the time traces of entropy generation caused by heat transfer, mass transfer, and chemical mechanisms during the particle gasification. The temporal variation of entropy generation by the stated three mechanisms is integrated over the part of the reactor in which there exit temperature species gradients. It is observed that the different sources of irreversibility share the same order of magnitude except for the condition that the initial particle temperature is 1000K. Further, the qualitative behaviours of the sources of irreversibility are quite similar. The endothermic devolatilisation process causes the temperature difference in the reactor and the thermal source of irreversibility appears at the very beginning. Once the volatile is released through the devolatilisation, the mass transfer entropy is generated by the diffusion of species to the surroundings. The chemical entropy generation takes place when the char reaction (R2) occurs. It needs to be pointed out that the thermal entropy is about five orders of magnitude smaller than the mass and chemical entropy when the particle temperature is 1000K. This corresponds to the result presented in Fig. 7 where the average rate of entropy generation at the particle temperature of 1000K can be ignored. The higher the temperature of the particle is, the earlier the peak of the mass transfer entropy generation and the greater peak value appears. The chemical source of irreversibility experiences a rising process in all investigated cases and the duration of the rising process is influenced by the particle temperature. The higher particle temperature results in a shorter rising process. Further, entropy generation by the chemical mechanisms declines along with the depletion of the biomass particle and the completion of the transient gasification process.

Figures 9 and 10 illustrate the spatiotemporal evolutions of entropy generated by heat and mass transfer as well as chemical reactions for the selected instances of time and varying particle initial temperatures. The horizontal axis of the subfigures represents the radial distance from the reactor centreline, and the vertical axis represents the downward vertical distance from the particle releasing point. Figure 9 shows that, prior to the char reaction, the irreversibility from the chemical mechanisms is zero, while there was a finite value for the sources of irreversibility by heat and mass transfer. Due to the endothermic devolatilisation, there is a distribution of thermal entropy along the particle travelling path. Diffusion of the produced volatile to the surrounding gaseous medium results in entropy generation by the mass transfer. This is the most significant contributor of the total entropy generation prior to the char reaction. As the gasification process continues, the spatial distribution of entropy generation by mass transfer further shows that there are two sources that contribute to it after the onset of char reaction. The first one close to the top of the reactor is resulted by the release and diffusion of the volatile from the devolatilisation process. The second source is in the vicinity of the particle and is caused by the production and diffusion of CO from the char reaction (R2). A comparison between the two sources shows that the second source of irreversibility is much smaller. This is mainly due to the lower generation of CO than that of volatile which has been indicated with the values of concentrations in Figs. 5 and 6. As depicted by Fig. 10, the slow mass transfer of gaseous species in the late stage of the particle gasification also indicates the decrease of mass transfer irreversibility at different moments of time. The generation of chemical entropy appears clearly after the initiation of char reactions. It is important to note that, the chemical source of irreversibility maintains a high value for a relatively long time while the entropy generation by heat and mass transfer decreases rapidly from the peak moment. This result is also reflected by the average entropy generation rates of the whole process (Fig. 7) and the history of the entropy generation (Fig. 8).

Figure 10 reports the spatial distribution of entropy generation by heat and mass transfer and chemical reactions when the particle temperature increases to 1000K. It can be seen that the increase of particle temperature has shown no qualitative changes in the entropy generations. However, compared with those in the corresponding subfigures of Fig. 9, the values of entropy generation from mass transfer and chemical reactions increase while that from heat transfer decreases significantly. Once again, this indicates that the mass transfer and chemical sources of irreversibility dominate the generation of entropy under higher temperature conditions, which is consistent with the results shown in Figs. 7 and 8.

It is finally emphasised that the temperature dependency of gasification makes entropy generation a function of temperature. Here, the analysis was conducted at constant reactor temperature of 1000K and only the effects of the initial temperature of the particle were investigated. It remains as a future task to explore the effects of different gasification temperatures upon the entropic behaviours of the process.

5. Conclusions

Aiming at provision of a systematic investigation of the gasification of a single biomass particle in CO_2 atmospheres, an equilibrium model was developed and validated against the reference data. Syngas production, carbon, and CO_2 conversion rates and energy efficiencies obtained from the analyses were subsequently analysed. Further, an axisymmetric CFD model was established to simulate the gasification process. Through using this model, the transient evolutions of the chemical species and gas temperature as well as those of entropy generations were investigated. The main results of this study are summarised below.

- For a given gasification temperature, as the moisture content in the feedstock increases, the production of CO, the lower heating value of the syngas and the energy and exergy efficiencies decrease while the production of H_2 increases. However, the increasing C/CO_2 ratio promotes the CO and H_2 generation, which then leads to improvement of the gasification performance.
- When the moisture content in the biomass is fixed, the syngas production, the carbon, and CO_2 conversion rate and the efficiencies feature the same trend. All these values increase when the gasification temperature or the C/CO_2 ratio increases, and they are more sensitive to the C/CO_2 ratio variations than the gasification temperature.
- The spatiotemporal variations of the gaseous species (CO, CO_2 and volatile) indicate that the particle temperature has a significant effect on the completion and duration of the gasification process. The higher particle temperatures promote the chemical reaction rate and consequently, shorten the gasification process significantly.
- Entropy generation by chemical reactions is the dominant contributor to the total entropy generation during the CO_2 gasification of biomass particles. The higher particle temperatures tend to substantiate the average rate of chemical entropy generation. However, the thermal source of irreversibility declines when the temperature difference between the reactor and particles becomes smaller, and it is practically negligible compared to the entropy generation by the mass transfer and chemical reactions.

Appendix A. Derivation of unsteady entropy generation

The unsteady entropy generation model is on the basis of the governing equations and Gibbs equation [49]. It can be derived by following the steps below:

Firstly, the equations representing the conservation of mass, energy and chemical species in the CFD model of this study are the followings:

$$\frac{\partial \rho}{\partial t} + \frac{\partial}{\partial x}(\rho u_x) + \frac{\partial}{\partial r}(\rho u_r) + \frac{\rho u_r}{r} = 0. \qquad (A1)$$

$$\frac{\partial(\rho h')}{\partial t}+\frac{\partial(\rho h' u_r)}{\partial r}+\frac{\partial(\rho h' u_x)}{\partial x}=\frac{\partial p}{\partial t}-\frac{\partial q_j}{\partial(x,r)}+Q_r, \tag{A2}$$

$$\frac{\partial(\rho Y_i)}{\partial t}+\frac{\partial(\rho Y_i u_r)}{\partial r}+\frac{\partial(\rho Y_i u_x)}{\partial x}=\frac{\partial\left(J_{i,j}\right)}{\partial(x,r)}+R_i, \tag{A3}$$

Considering the entropy generation in the gas-phase of the gasification process, the Gibbs equation here is expressed by:

$$Tds=du+pd\left(\frac{1}{\rho}\right)-\sum_i \mu_{c,i}dY_i. \tag{A4}$$

An algebraic manipulation of Eq. (A4) is written as,

$$T\frac{\partial s}{\partial t}=\frac{\partial u}{\partial t}-\frac{p}{\rho^2}\frac{\partial \rho}{\partial t}-\sum_i \overline{\mu_{c,i}}\frac{\partial Y_i}{\partial t}, \tag{A5}$$

in which $\mu_{c,i}=\overline{\mu_{c,i}}/M_i$ is the specific chemical potential.

By substituting the conservation equations Eqs. (A1) -(A3) into the Eq. (A5) and multiplying the result by ρ/T , it gives:

$$\rho\frac{\partial s}{\partial t}=-\frac{1}{T}\nabla\cdot\vec{q}+\frac{\Phi}{T}+\frac{\rho}{T}\sum_i Y_i\vec{f_i}\cdot\vec{V_i}-\frac{1}{T}\sum_i \mu_{c,i}\left[\omega_i-\nabla\cdot\left(\rho Y_i\vec{V_i}\right)\right], \tag{A5}$$

Then, it can be then reformulated as

$$\begin{aligned}\rho\frac{\partial s}{\partial t}=&-\nabla\cdot\left[\left(\frac{\vec{q}}{T}\right)-\frac{1}{T}\sum_i \mu_{c,i}\rho Y_i\vec{V_i}\right]-\frac{\vec{q}}{T^2}\cdot\nabla T+\frac{\Phi}{T}+\frac{\rho}{T}\sum_i Y_i\vec{f_i}\cdot\vec{V_i}\\&-\frac{1}{T}\sum_i \mu_{c,i}\omega_i+\frac{1}{T^2}\sum_i \mu_{c,i}\rho Y_i\vec{V_i}\cdot\nabla T-\frac{1}{T}\sum_i \rho Y_i\vec{V_i}\cdot\nabla\left(\mu_{c,i}\right).\end{aligned} \tag{A7}$$

The entropy flux is obtained from Ref. [50] when considering the entropy change:

$$\vec{s}=\left(\frac{\vec{q}}{T}\right)-\frac{1}{T}\sum_i \mu_{c,i}\rho Y_i\vec{V_i}. \tag{A8}$$

and

$$\sigma=-\frac{\vec{q}}{T^2}\cdot\nabla T+\frac{\Phi}{T}+\frac{\rho}{T}\sum_i Y_i\vec{f_i}\cdot\vec{V_i}-\frac{1}{T}\sum_i \mu_{c,i}\omega_i+\frac{1}{T^2}\sum_i\left(\mu_{c,i}\rho Y_i\vec{V_i}\right)\cdot\nabla T-\frac{1}{T}\sum_i \rho Y_i\vec{V_i}\cdot\nabla\left(\mu_{c,i}\right). \tag{A9}$$

Equation (A9) can be converted into a form similar to that given by Carrington and Sun [51]:

$$\sigma=-\frac{\vec{q}}{T^2}\cdot\nabla T+\frac{\Phi}{T}+\frac{1}{T}\sum_i \rho Y_i\vec{V_i}\cdot\left(\vec{f_i}+\frac{\mu_{c,i}}{T}\nabla T-\nabla\mu_{c,i}\right)-\frac{1}{T}\sum_i \mu_{c,i}\omega_i. \tag{A10}$$

Here, $\vec{q}$ is defined as the total heat flux and is expressed by:

$$\vec{q}=-\lambda\cdot\nabla T+\rho\sum Y_i\vec{V_i}h_i, \tag{A11}$$

Give the assumption that ignoring the irreversibility caused by the viscous dissipation [52]. Here are:

$$\mu_{c,i} = h_i - Ts_i, \tag{A12}$$

$$s_i = s_i^0 + \int_{T^0}^{T} \frac{c_{p,i}}{T} dT - \frac{R_u}{M_i} ln\left(\frac{p}{p^0}\right) - \frac{R_u}{M_i} lnX_i, \tag{A13}$$

$$\nabla X_i = \sum_{\substack{j=1 \\ j\neq i}}^{N} \left(\frac{X_i X_j}{D_{ij}}\right)\left(\vec{V_j} - \vec{V_i}\right) + \sum_{\substack{j=1 \\ j\neq i}}^{N} \left(\frac{X_i X_j}{D_{ij}}\right)\left(\frac{D_{T,j}}{\rho_j} - \frac{D_{T,i}}{\rho_i}\right)\left(\frac{\nabla T}{T}\right). \tag{A14}$$

Combining the equations Eqs. (A11)-(A14), the entropy generation of the process can be written in the following form:

$$\sigma = \frac{\lambda}{T^2}(\nabla T)^2 + \frac{\rho R_u D_{im}}{\bar{M}} \frac{1}{X_i} (\nabla X_i)^2 - \frac{1}{T} \sum_i \mu_{c,i} \omega_i. \tag{A15}$$

Therefore, the rate of entropy generation caused by heat transfer (E_h), mass transfer (E_m), and chemical reactions (E_r) can be obtained from the right-hand side of the equation.

$$E_h = \frac{\lambda}{T^2}(\nabla T)^2, \tag{A16a}$$

$$E_m = \frac{\rho R_u D_{im}}{\bar{M}} \frac{1}{X_i} (\nabla X_i)^2, \tag{A16b}$$

$$E_r = -\frac{1}{T} \sum_i \mu_{c,i} \omega_i. \tag{A16c}$$

Acknowledgment

The last author would like to acknowledge his RAEng/The Leverhulme Trust Senior Research Fellowship (LTSRF1718\14\45) provided by the Royal Academy of Engineering.

References

[1] Stassesn HEM. Biogas and biomass technology: energy generation from biomass. World Renewable Energy Conference, Reading, 1994.

[2] Basu P. Biomass gasification and pyrolysis: Practical design and theory. Elsevier. 2010.

[3] Wang LW, Karimi N, Sutardi T, Paul MC. Combustion Characteristics and Pollutant Emissions in Transient Oxy-Combustion of a Single Biomass Particle: A Numerical Study. Energy & Fuels, 2019, 33(2), 1556-1569.

[4] Salem A, Paul MC. An integrated kinetic model for downdraft gasifier based on a novel approach that optimises the reduction zone of gasifier. Biomass and Bioenergy, 2018, 109, 172-181.

[5] Kumar U, Paul MC. CFD modelling of biomass gasification with a volatile break-up approach. Chemical Engineering Science, 2019, 195, 413-422.

[6] Kirkels AF, Verbong GPJ. Biomass gasification: Still promising? A 30-year global overview. Renewable and Sustainable Energy Reviews, 2011, 15(1), 471-481.

[7] Hosseini M, Dincer I, Rosen MA. Steam and air fed biomass gasification: Comparisons based on energy and exergy. Renewable and Sustainable Energy Reviews, 2012, 37(21), 16446-16452.

[8] Ruiz JA, Juarez MC, Morales MP, Munoz P, Mendivil MA. Biomass gasification for electricity generation: Review of current technology barriers. Renewable and Sustainable Energy Reviews, 2013, 18, 174-183.

[9] Hosseini SE, Wahid MA. Hydrogen production from renewable and sustainable energy resources: Promising green energy carrier for clean development. Renewable and Sustainable Energy Reviews, 2016, 57, 850-866.

[10] Sutardi T, Paul MC, Karimi, N. Investigation of coal particle gasification processes with application leading to underground coal gasification. Fuel, 2019, 237, 1186-1202.

[11] Sutardi T, Wang LW, Karimi N, Paul MC. Utilization of H2O and CO2 in Coal Particle Gasification with an Impact of Temperature and Particle Size. Energy & Fuels, 2020, 34(10), 12841-12852.

[12] Chaiwatanodom P, Vivanpatarakij S, Assabumrungrat S. Thermodynamic analysis of biomass gasification with CO_2 recycle for synthesis gas production. Applied Energy, 2014, 114, 10-17.

[13] Prabowo B, Aziz M, Umeki K, Susanto H, Yan M, Yoshikawa K. CO_2-recycling biomass gasification system for highly efficient and carbon-negative power generation. Applied Energy, 2015, 158, 97-106.

[14] Chen W, Thanapal. SS, Annamalai K, Ansley RJ, Mirik M. Updraft gasification of mesquite fuel using air/steam and CO_2/O_2 mixtures. Energy & Fuels, 2013: 27, 7460-7469.

[15] Mathieu P, Dubuisson R. Performance analysis of a biomass gasifier. Energy Conversion and Management, 2002, 43, 1291-1299.

[16] Im-orb K, Simasatitkul L, Arpornwichanop A. Analysis of synthesis gas production with a flexible H_2/CO ratio from rice straw gasification. Fuel, 2016, 164, 361-373.

[17] Sadhwani N, Adhikari S, Eden MR. Biomass gasification using carbon dioxide: Effect of temperature, CO_2/C ratio, and the study of reactions influencing the process. Industrial & Engineering Chemistry Research, 2016, 55, 2883-2891.

[18] Parvez AM, Mujtaba IM, Wu T. Energy, exergy and environmental analysis of conventional, steam and CO_2-enhanced rice straw gasification. Energy, 2016, 94, 579-588.

[19] Ptasinski KJ, Prins MJ, Pierik A. Exergetic evaluation of biomass gasification. Energy, 2007, 32, 568-574.

[20] Karamarkovic R, Karamarkovic V. Energy and energy analysis of biomass gasification at different temperatures. Energy, 2010, 35, 537-549.

[21] Kazemian Y, Rashidi S, Esfahani JA, Samimi-Abianeh O. Effects of grains shapes of porous media on combustion onset – A numerical simulation using Lattice Boltzmann method. Computers & Mathematics with Applications, 2021, 81(1), 547-561.

[22] Rashidi S, Hormozi F, Doranehgard MH. Abilities of porous materials for energy saving in advanced thermal systems. Journal of Thermal Analysis and Calorimetry, 2021, 14, 2437-2452.

[23] Kazemian Y, Rashidi S, Esfahani JA, Karimi N. Simulation of conjugate radiation-forced convection heat transfer in a porous medium using the lattice Boltzmann method. Meccanica, 2019, 54, 505-524.

[24] Al-Shemmeri T. Engineering Thermodynamics. Ventus Publishing APS. 2010.

[25] Bejan A. Advanced Engineering Thermodynamics. John Wiley & Sons, 2016.

[26] Torabi M, Karimi N, Torabi M, Peterson GP, Simonson CJ. Generation of entropy in micro thermofluidic and thermochemical energy systems-A critical review. International Journal of Heat and Mass Transfer, 2020, 163, 120471.

[27] Hunt G, Torabi M, Govone L, Karimi N, Mehdizadeh A. Two-dimensional heat and mass transfer and thermodynamic analyses of porous microreactors with Soret and thermal radiation effects—an analytical approach. Chemical Engineering and Processing-Process Intensification, 2018, 126, 190-205.

[28] Wang W, Zuo Z, Liu J, Yang W. Entropy generation analysis of fuel premixed CH_4/H_2/air flames using multistep kinetics. International Journal of Hydrogen Energy, 2016, 41(45), 20744-20752.

[29] Som SK, Mondal SS, Dash SK. Energy and exergy balance in the process of pulverized coal combustion in a tubular combustor, Journal of Heat Transfer, 2005, 127(12), 1322-1333.

[30] Prins MJ, Ptasinski KJ, Janssen FJJG. From coal to biomass gasification: Comparison of thermodynamic efficiency. Energy, 2007, 32, 1248-1259.

[31] Florin NH, Harris AT. Enhanced hydrogen production from biomass with in situ carbon dioxide capture using calcium oxide sorbents. Chemical Engineering Science, 2008, 63, 287-316.

[32] Mountouris A, Voutsas E, Tassios D. Solid waste plasma gasification: Equilibrium model development and exergy analysis. Energy Conversion and Management, 2006, 47, 1723-1737.

[33] Prins MJ, Ptasins KJ, Janssen FJJG. From coal to biomass gasification: comparison of thermodynamic efficiency. Energy, 2007, 32(7), 1248-1259.

[34] Zainal ZA, Ali R, Lean CH et al. Prediction of performance of a downdraft gasifier using equilibrium modeling for different biomass materials. Energy Conversion and Management, 2001, 42, 1499-1515.

[35] Zhang X, Wang A, Arellano-Garcia H, Wozny G. Performances Evaluation of Biomass Gasification and Synthetic Gas Co-Firing in Coal-Fired Boiler, 2011 Asia-Pacific Power and Energy Engineering Conference, Wuhan, China, 2011, pp. 1-4

[36] Gonzalez AM, Lora EES, Palacia JCE. Syngas production from oil sludge gasification and its potential use in power generation systems: An energy and exergy analysis. Energy, 2019, 169, 1175-1190.

[37] Zhang Q, Wu Y, Dor L, Yang W, Blasiak W. A thermodynamic analysis of solid waste gasification in the Plasma Gasification Melting process. Applied Energy, 2013, 112, 405-413.

[38] Wang LW, Karimi N, Paul MC. Gas-phase transport and entropy generation during transient combustion of single biomass particle in varying oxygen and nitrogen atmospheres. International Journal of Hydrogen Energy, 2018, 43, 8506-8523.

[39] Wang LW, Karimi N, Sutardi T, Paul MC. Numerical modelling of unsteady transport and entropy generation in oxy-combustion of single coal particles with varying flow velocities and oxygen concentrations. Applied Thermal Engineering, 2018, 144, 147-164.

[40] ANSYS Fluent Theory guide15.0. 2013.

[41] Blaid S, Paul MC, Watson IA. Numerical investigation of the heterogeneous combustion processes of solid fuels. Fuel, 2015, 141, 236-249.

[42] Mayers AM. The rate of reduction of carbon dioxide by graphite. Journal of the American Chemical Society, 1934, 56(1), 70-76.

[43] Ahmed I. Gupta AK. Characteristics of cardboard and paper gasification with CO_2. Applied Energy, 2009, 86, 2626-2634.

[44] Hu YY, Yu HQ, Zhou FL, Chen DZ. A comparison between CO2 gasification of various biomass chars and coal char. The Canadian Journal of Chemical Engineering, 2018, 9999, 1-6.

[45] Sepe AM, Li J, Paul MC. Assessing biomass steam gasification technologies using a multi-purpose model. Energy Conversion and Management, 2016, 129, 216-226.

[46] Salem AM, Paul MC. An integrated kinetic model for downdraft gasifier based on a novel approach that optimises the reduction zone of gasifier. Biomass and Bioenergy, 2018, 109, 172-181.

[47] Nishida K, Takagi T, Kinoshita S. Analysis of entropy generation and exergy loss during combustion. Proceedings of the Combustion Institute, 2002, 29(1), 869-874.

[48] Jiang DY, Yang WM, Chua KJ. Entropy generation analysis of H_2/air premixed flame in micro-combustors with heat recuperation. Chemical Engineering Science, 2013, 98, 265-272.

[49] Williams FA. Combustion Theory, second ed. Benjamin/Cummings, Menlo Park, California, 1985.

[50] Hirschfelder JO, Curtiss CF, Bird RB. Molecular Theory of Gases and Liquids. Wiley, New York, 1954.

[51] Carrington CG, Sun ZF. Second law analysis of combined heat and mass transfer phenomena. International Journal of Heat and Mass Transfer, 1991, 34(11):2767-2773.

[52] Köser J, Becker LG, Vorobiev N, Schiemann M, Scherer V, Böhm B, Dreizler A. Characterization of single coal particle combustion within oxygen-enriched environments using high-speed OH-PLIF. Applied Physics B, 2015, 121(4): 459-464.

Figures

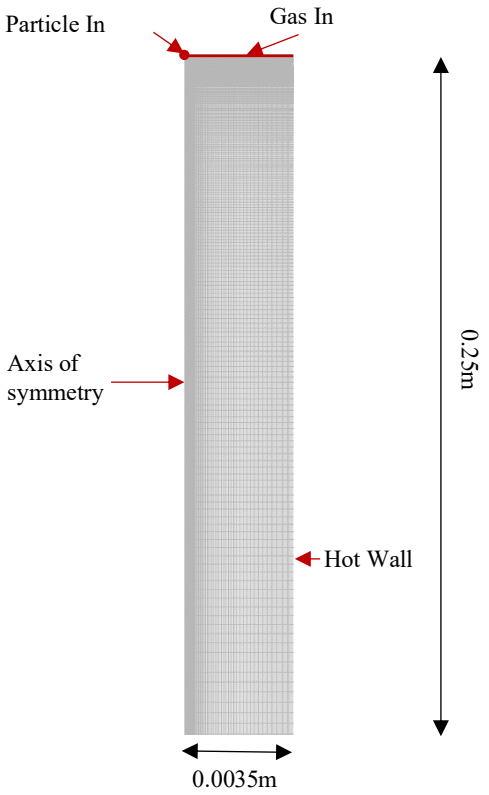

Figure. 1: Schematic view of the computational domain.

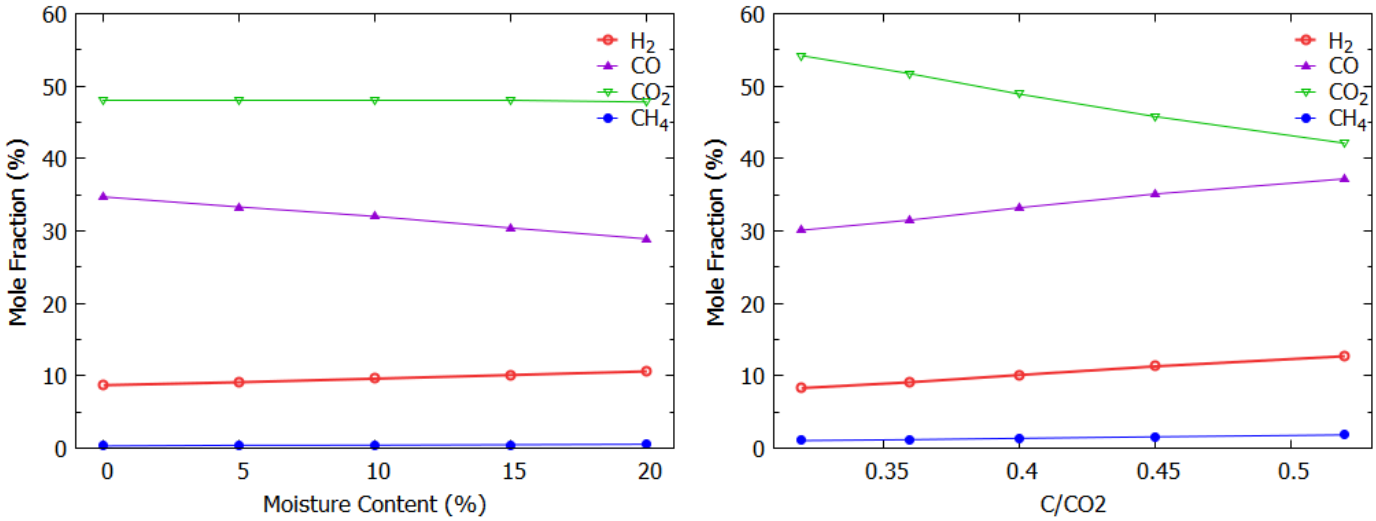

a. varying moisture content in feedstock (C/CO_2=0.32). b. varying C/CO_2 ratio (moisture content=0.96%).

Figure 2. Syngas production under varying conditions when gasification temperature is 1000K.

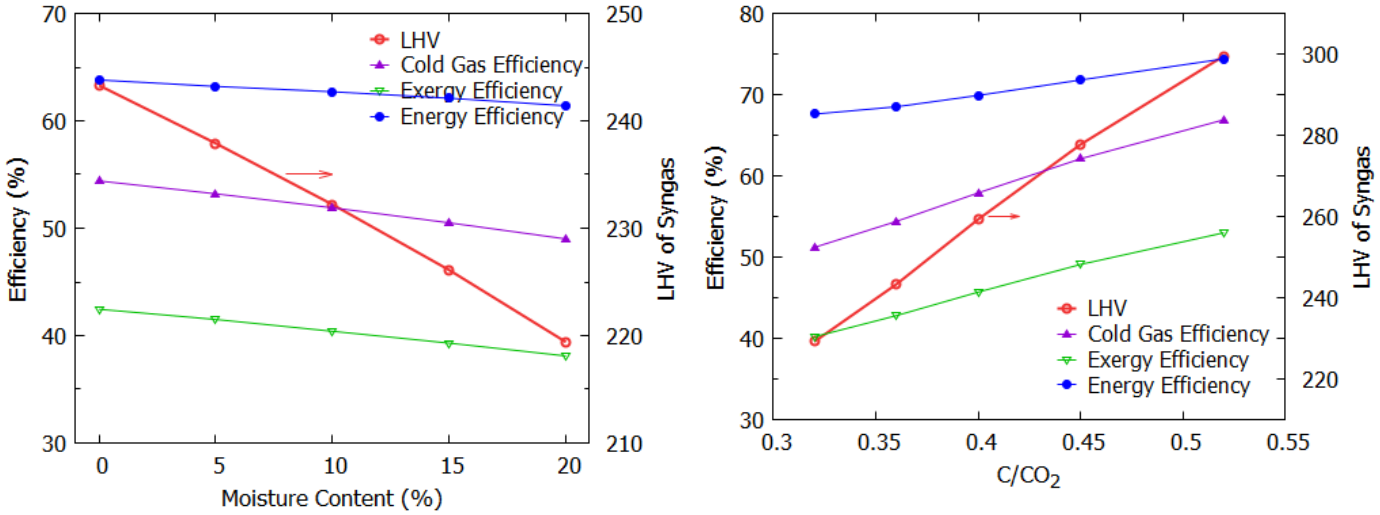

a. varying moisture content in feedstock (C/CO_2=0.32). b. varying C/CO_2 ratio (moisture content=0.96%).

Figure 3. Gasification efficiencies and LHV (kJ/mol) of syngas under varying conditions when gasification temperature is 1000K.

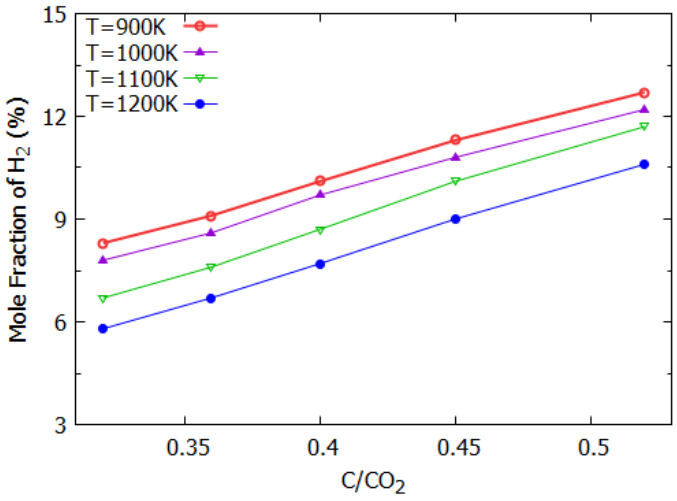

a. H_2 production

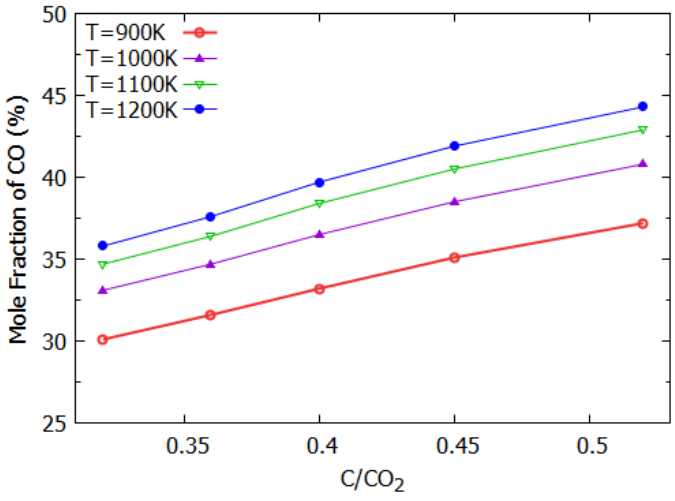

b. CO production

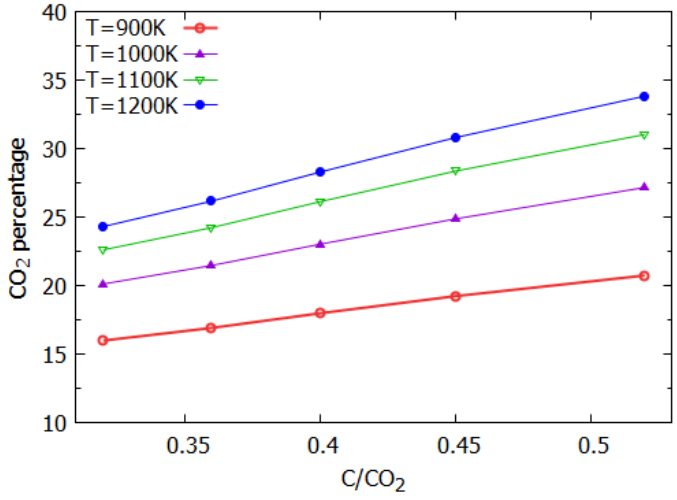

c. CO_2 reduction rate

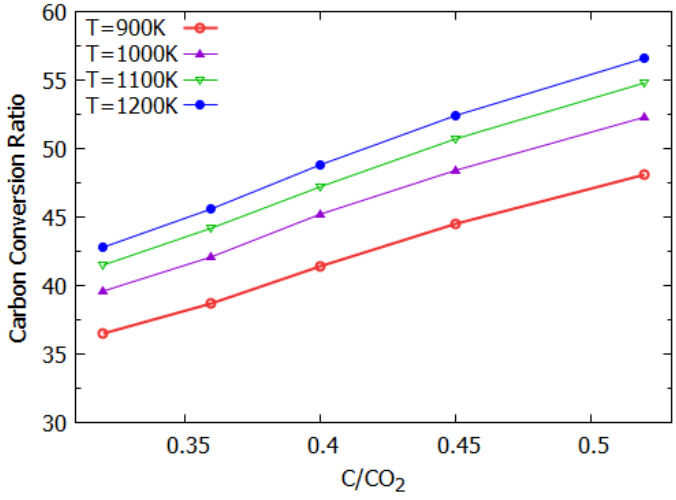

d. carbon conversion rate

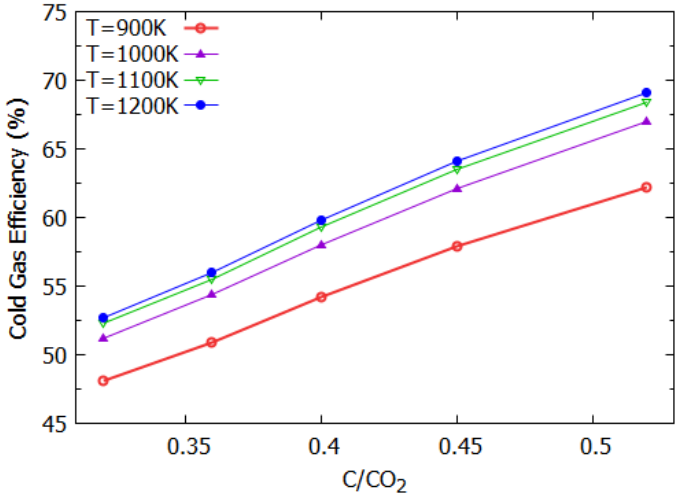

e. cold gas efficiency

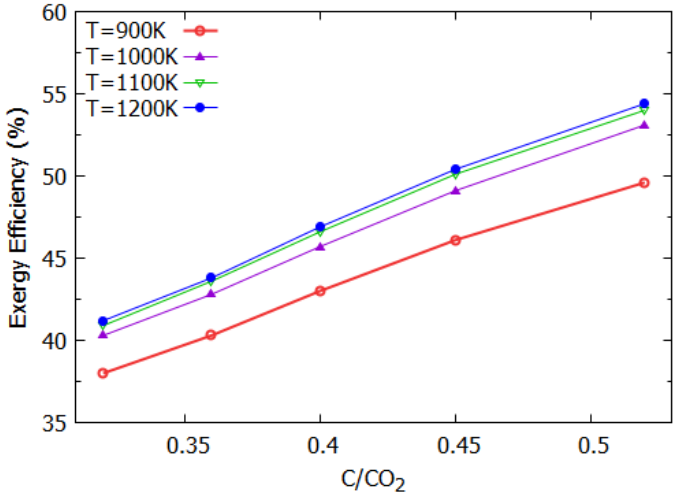

f. exergy efficiency

Figure 4. Effect of C/CO_2 ratio on biomass gasification when the gasification temperature varies (moisture content=0.96%).

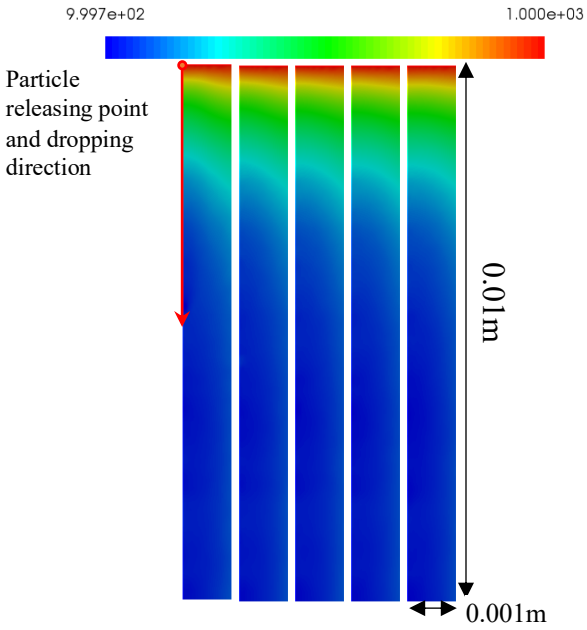

a. Evolution of gas-phase temperature.

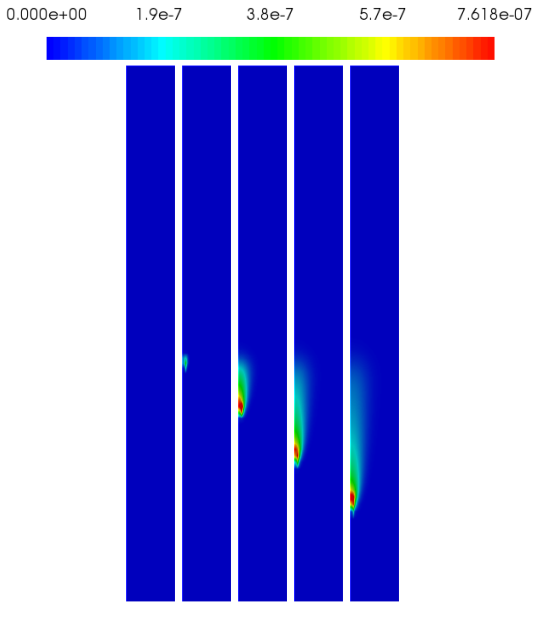

b. Evolution of mole fraction of CO.

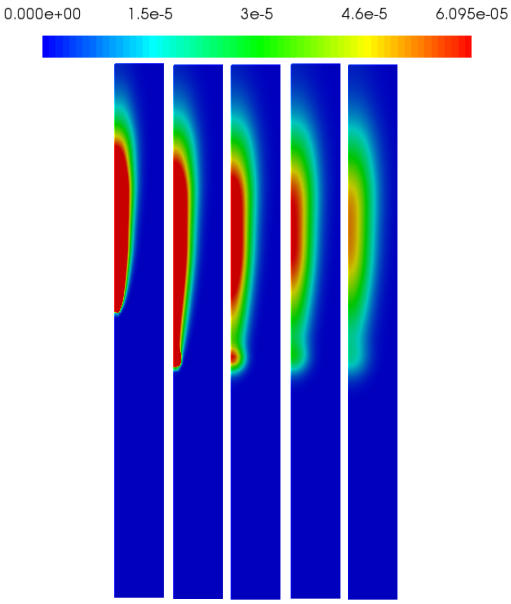

c. Evolution of mole fraction of volatile.

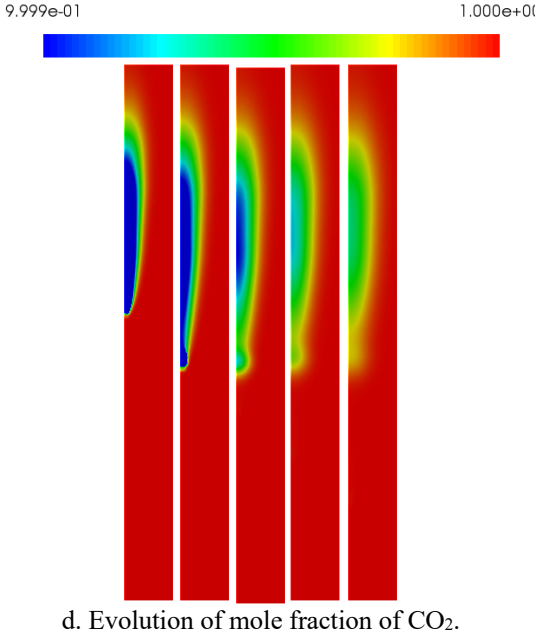

d. Evolution of mole fraction of CO_2.

Figure 5. Spatiotemporal evolution of biomass gasification process when particle temperature is 500K (130ms, 160ms, 190ms, 220ms, 250ms).

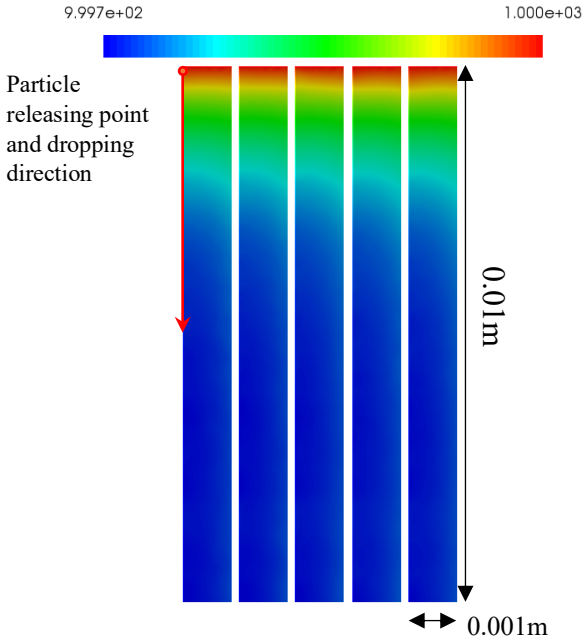

a. Evolution of gas-phase temperature.

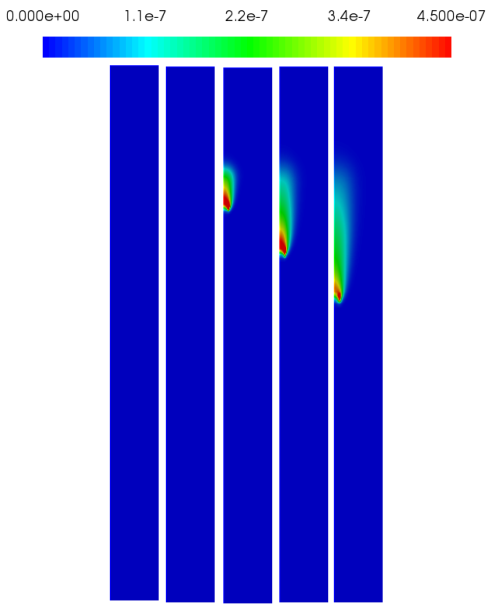

b. Evolution of mole fraction of CO.

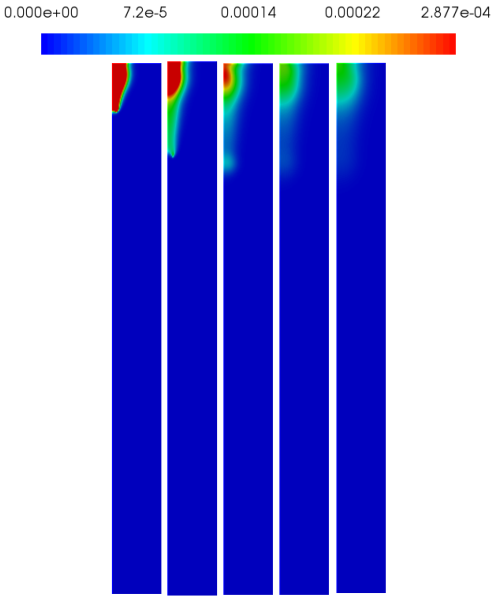

c. Evolution of mole fraction of volatile.

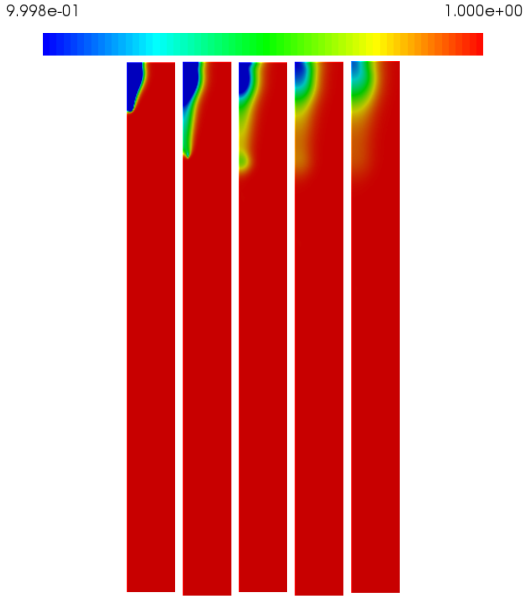

d. Evolution of mole fraction of CO_2.

Figure 6. Spatiotemporal evolution of biomass gasification process when particle temperature is 1000K (40ms, 70ms, 100ms, 130ms, 160ms).

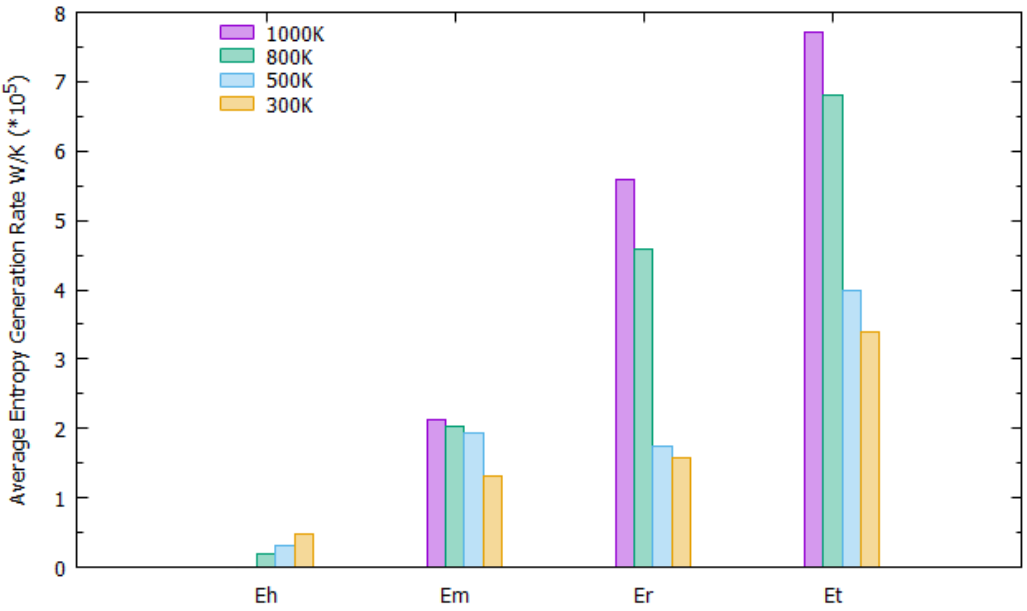

Figure 7. Compared total generation of entropy under various particle temperature conditions.

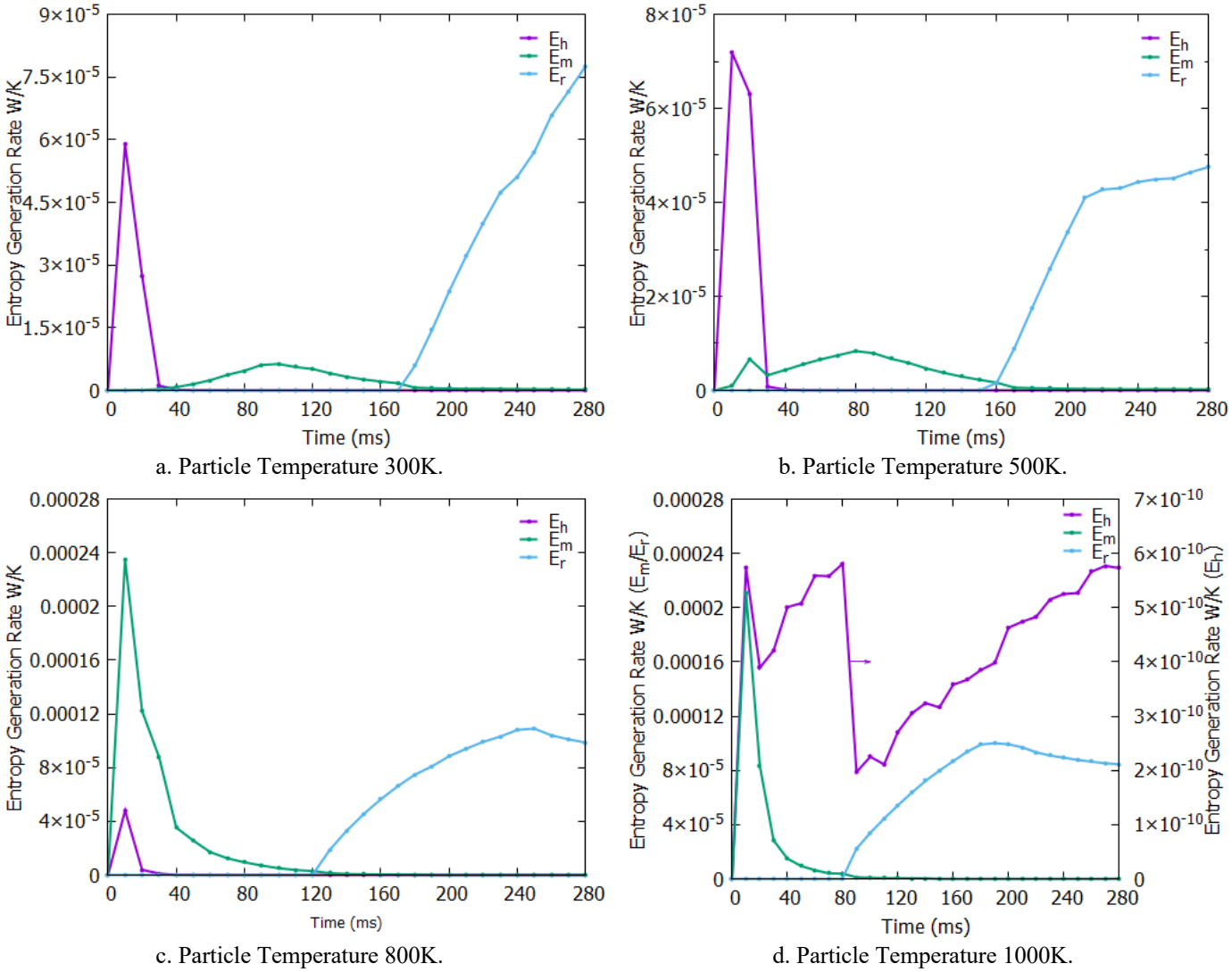

a. Particle Temperature 300K.

b. Particle Temperature 500K.

c. Particle Temperature 800K.

d. Particle Temperature 1000K.

Figure 8. History of entropy generation by different sources of irreversibility.

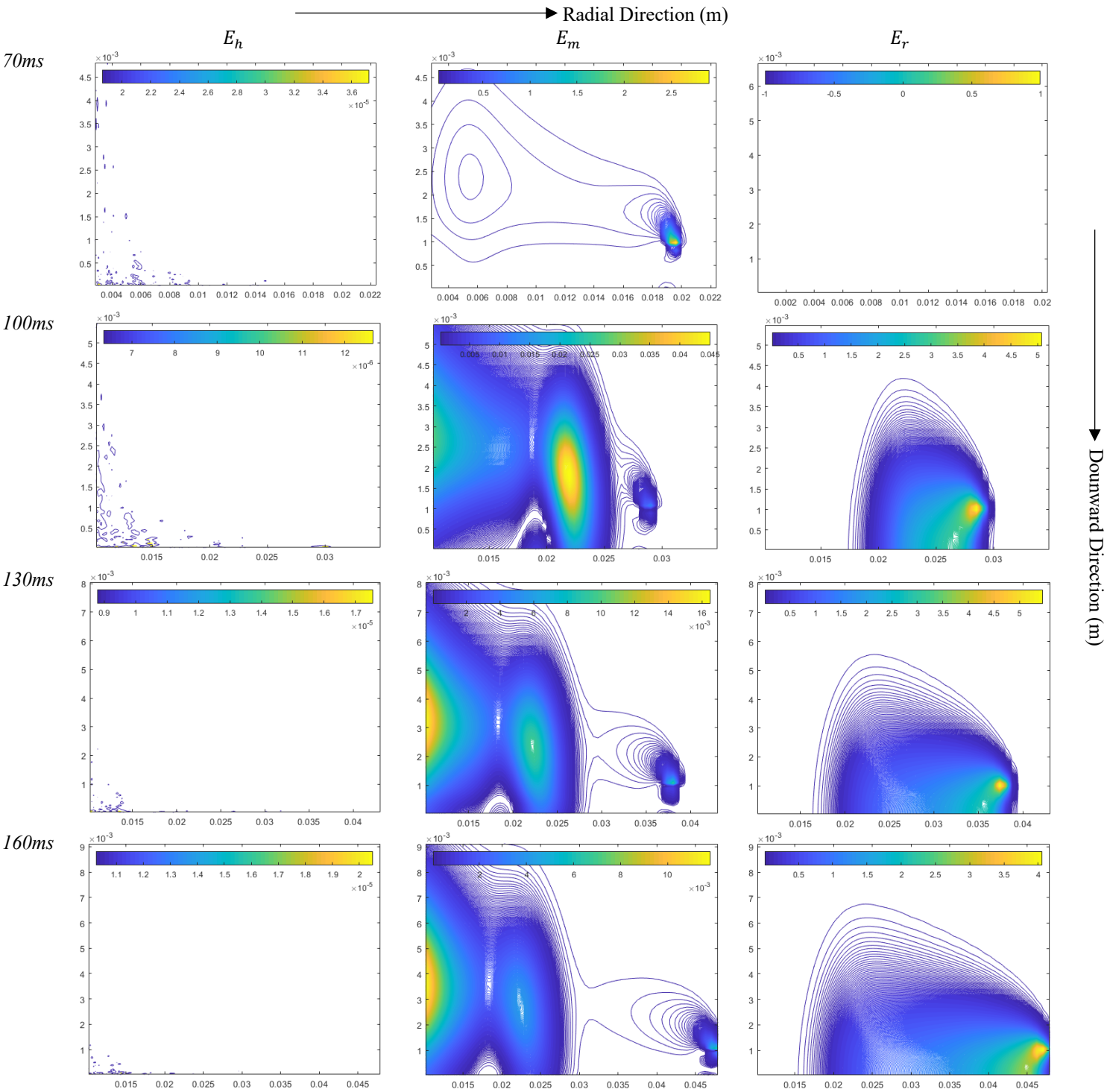

Figure 9. Spatiotemporal evolution of entropy generation rate per unit volume (W/m^{2}K) under particle temperature of 1000K.

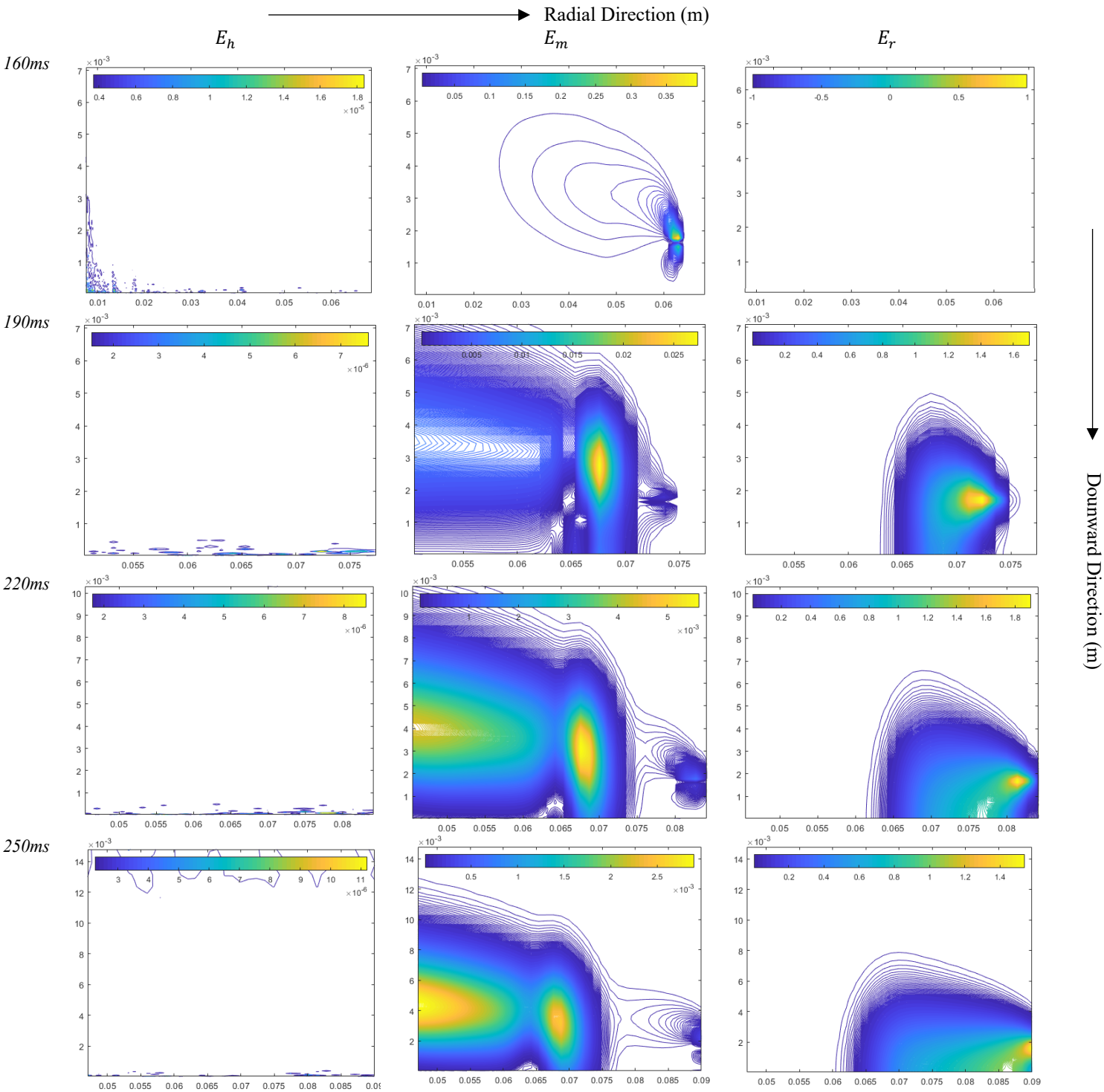

Figure 10. Spatiotemporal evolution of entropy generation rate per unit volume (W/m^{2}K) under particle temperature of 300K.